RESEARCH PAPER

Graphite-Enhanced TiO_2 Nanoparticles Protect Duplex Stainless Steel against Acidic Corrosion

Mohammad N. Majeed [1], *Qahtan. A. Yousif* [2] *

[1] University of Al- Qadisiyah, College of education, Department of chemistry, Iraq

[2] University of Al- Qadisiyah, College of engineering, Department of materials engineering, Iraq

ARTICLE INFO

Article History:
Received 22 March 2022
Accepted 19 June 2022
Published 01 July 2022

Keywords:
Coating
Corrosion
DSS
Graphite
Protection
TiO_2

ABSTRACT

In this work, TiO_2 nanoparticles with graphite are used to coat duplex stainless steel (DSS) using the negative electrodeposition technique to protect it from corrosion. The anticorrosion performance of nanoparticle coatings that comprised a proper quantity of graphite particles was investigated using an open circuit potential and a potentiodynamic technique in a 1 M H_2SO_4 solution saturated with carbon dioxide. The corrosion rate of the DSS sample was lower when it was coated with TiO_2/graphite than when it was uncoated, and the potential for corrosion increased from - 0.450 V for the uncoated DSS surface to - 0.410 V for the saturated calomel when it was coated with TiO_2/graphite. Electrochemical studies discovered that TiO_2/graphite coated DSS corrosion in sulfuric acid media had excellent protective qualities, with an effectiveness of 77.74 % when the current density was 0.957 milliamps per centimeter squared. It has been established by the findings of this study that duplex stainless steel can be protected against corrosion in acidic conditions by the application of protective coating layers. The surface morphology of TiO_2/graphite coating has demonstrated that it may withstand an acid attack due to its high adherence to the surface sample. X-ray diffraction was used to improve the accuracy of measurements for determining and researching the composition of the alloy surface's protective layer.

How to cite this article
Majeed M N, Yousif Q A. Graphite-Enhanced TiO_2 Nanoparticles Protect Duplex Stainless Steel against Acidic Corrosion. J Nanostruct, 2022; 12(3):616-624. DOI: 10.22052/JNS.2022.03.015

INTRODUCTION

Stainless steels are an essential group of engineering alloys that have been used in a wide range of things, from household appliances to parts for spacecraft. Because of their austenitic and ferritic grains, duplex stainless steels (DSSs) can be very useful [1,2]. DSSs have higher toughness and weldability than ferritic ones [3–5]. DSSs are more resistant to pitting and stress corrosion cracking than austenitic grades [6]. As a result, they are widely utilized in the chemical, petrochemical, culinary, electricity, transportation, pulp and paper, and oil refinery industries. DSSs have higher toughness and weldability than ferritic ones [7,8]. DSSs are more resistant to pitting and stress corrosion cracking than austenitic grades [9]. DSSs have strong corrosion resistance due to their high Cr content combined with significant additions of Mo, Ni, and N. Chromium adds to stainless steel corrosion resistance by producing protective Cr-oxide or hydroxide in the passive coating [10-12]. Due to the creation of a passive protective coating, stainless steels have a wide range of industrial uses due to their corrosion resistance [13].

* Corresponding Author Email: qahtan.adnan@qu.edu.iq

Chromium and other major alloying elements are to blame for this film. As sulfate anions are present, they destabilize at sites or regions of inclusions, impurities, grain boundaries, and other faults that cause localized corrosion [14]. Because of chromium and other essential alloying elements, this film exists. It destabilizes in the presence of aggressive sulfate anions, particularly at inclusions, impurities, grain boundaries, and other imperfections that cause localized corrosion. Sulfuric acid, the world's most essential and frequently used industrial chemical, is the primary source of corrosive sulfates [15,16]. Its corrosivity to stainless steel alloys varies according to concentration and alloy type [17]. The majority of sulfuric acid encountered is in diluted proportions for various chemical processes, including mineral processing, petroleum production, and water treatment [16,18]. Alloy metals like nickel and chromium can be added to steel to increase corrosion and oxidation resistance, creating high-alloy steel like duplex stainless steel [19,20]. The use of corrosion-resistant materials is desirable in most circumstances where cost is considered [21]. Ferrous metals have long been protected against corrosion by applying corrosion inhibitors [22]. Electron-sharing and film-forming activity is the fundamental processes of inorganic corrosion inhibitors [23]. Organic coatings are commonly utilized in industry to protect metals from corrosion [24]. Ceramic coatings are also preferred over metal coatings because they are more resistant to oxidation, corrosion, erosion, and wear than metals in high-temperature conditions [25]. Nanoparticles are employed to improve hybrid sol-gel coatings' corrosion resistance and mechanical qualities [26-28]. Nanoparticles reduce fractures and porosity in nanocomposite coatings [29]. Nanoparticles can be introduced as a powder to coat materials or created during the creation of sol-gel coatings [30]. As a result, in this work, to improve the corrosion resistance of duplex stainless steel, we decided to take advantage of the beneficial features of nanoparticles, which were discovered through previous research. The DSSs were coated with titanium nanoparticles containing graphite (TiO_2/graphite) using a negative electrodeposition technique at a constant temperature. Electrochemical methods such as open circuit potential (OCP), and potentiodynamic (PD) were used to study the protection of DSSs at a constant temperature (298.15 K). Two surface morphology techniques, field emission scanning electron microscopy (FESEM) and energy-dispersive X-ray spectroscopy (EDS), were used to identify the nature of the coated surface. As a result, X-ray diffraction (XRD) was utilized in conjunction with the other tests, as it is a vital non-destructive technique for determining the alloy's protective film composition.

MATERIALS AND METHODS

Table 1 lists the components of the DSS samples. The following dimensions and thickness (2 cm x 2 cm) were used to build a piece (1 cm). Following polishing with emery sheets of varying diameters, all specimens were subsequently lubricated with diamond paste applied to an ultra-thin soft cloth. Sulfuric acid in deionized water saturated with carbon dioxide was utilized as an electrolyte solution to evaluate the protective effects of TiO_2 / graphite on the DSS electrode surface.

A TiO_2/graphite layer was electrodeposited on the DSS using a glass cell with a volume of 200 cm^3 and a DSSs electrode sandwiched between two parallel titanium metal electrodes. The electrodes were separated by 0.3 cm. The electrolyte, which contained 1.5 g/L TiO_2 and 0.5 g/L graphite, was agitated using a magnetic stirrer. The negative electrodeposition was performed for 2.5 minutes at a continuous DC voltage of 150 V, with the electrolyte held at 333.15 K. The samples were air-dried for 24 hours at room temperature before being stored in a desiccator until further testing. The corrosion electrochemical cell was coupled to a potentiostat device to determine comprehensive electrochemical parameters. FESEM (ZEISS Gemini, Germany, LTD. Company) was used to characterize specimens. The compositions of the chemical components were determined using EDS spectra. The XRD patterns were captured using the Bruker D6 Advanced diffraction system and a Cu

Table.1 Composition of DSS

Elements	C	Mn	Al	Si	Mo	Ni	Cr	Fe
Wt%	0.12	0.68	0.08	2.10	0.23	10.11	18.20	balance

radiation source.

RESULTS AND DISCUSSION

As a function of immersion time, the fluctuation can be used to determine the DSS coating in OCP. Fig. 1 illustrates the evolution of the open circuit potential with time for DSS in 1 M H_2SO_4 solution without and with coated protection. The curves demonstrate that the TiO_2/graphite protective layer significantly alters the temporal behaviour of the OCP. It is determined that it is a cathodic displacement of DSS in the absence of protection. However, when the cathodic (active) direction is protected by a TiO_2/graphite layer, the potential change in the cathodic (active) direction is more pronounced. OCP curve profiles with TiO_2/graphite coating exhibit typical anodic tendencies. On the other hand, the OCP values stayed steady in the latter case, moving slightly into the 1000s. This could indicate that a protective covering attaches to the surface of the DSS.

The polarization curves of an uncoated DSS and a TiO_2/graphite coated DSS are shown in Fig. 2. The corrosion potential (E_{corr}), the current

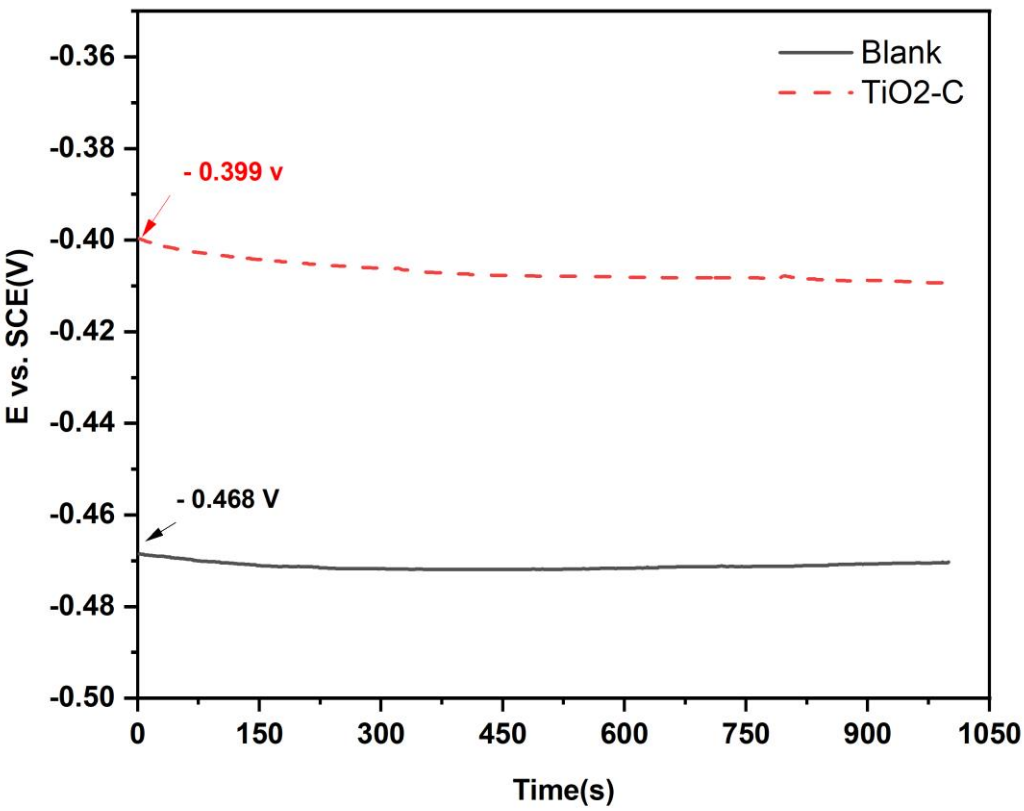

Fig. 1 OCP curves without and with coating layers of TiO_2/graphite on the DSS surface.

Table 2 Parameters of Potentiodynamic curves without and with coating layers of TiO_2/graphite on the DSS surface.

Type coating	$\beta a \times 10^{-3}$ (V/decade)	$\beta c \times 10^{-3}$ (V/decade)	i_{corr} (A/cm²)	E_{corr} (mV *vs.* SCE)	Corrosion Rate (mpy)	$\%\eta_{pr.}$
Blank	171.6	192.5	4.3×10^{-3}	-450.0	1.967×10^{3}	-
TiO_2-C	115.2	107.3	957×10^{-6}	-410.0	437.5	77.74

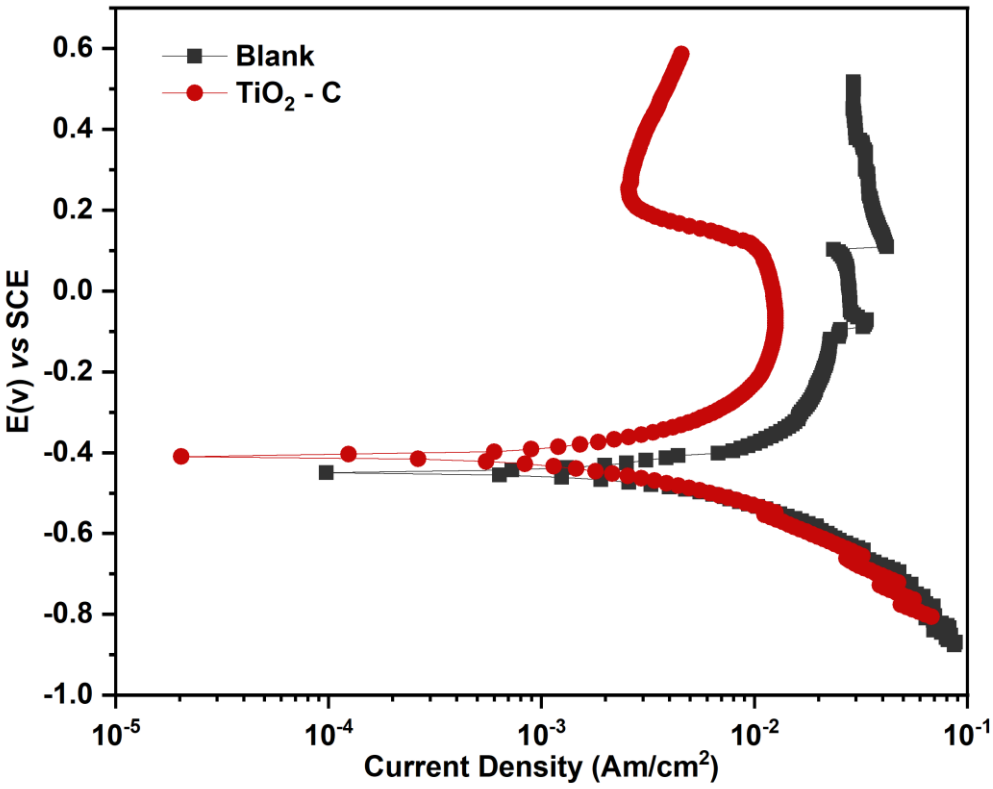

Fig. 2 Potentiodynamic curves without and with coating layers of TiO_2/graphite on the DSS surface.

density value (i_{corr}), the anodic Tafel constant (βa), the cathodic Tafel constant (βc), and the corrosion rate (CR) are all determined using these curves. The output of this calculation is summarized in Table 2. It was discovered that the coated specimen had a lower current density than the untreated DSS specimen. The coated sample's corrosion potential is changed from cathodic to anodic. This result indicates the coating's corrosive medium resilience. The following calculation can determine the percentage of protection efficiency based on corrosion current density measurements

Table 3 XRD analysis peaks of DSS surface and a coating layer of TiO_2/graphite.

Peak Position (2-theta)	FWHM (β)	Crystallite Size D (nm)	d-spacing (nm)	Intensity	Miller index
43.62	0.49	17.75	0.20	607	(111)
44.56	0.29	29.69	0.19	295	(110)
50.52	0.39	22.78	0.17	177	(200)
64.87	0.59	16.27	0.14	32	(200)
74.65	0.59	17.27	0.12	89	(220)
TiO_2/graphite					
27.58	0.29	28.28	0.31	59	(110)
36.17	0.59	14.45	0.24	29	(101)
43.65	0.34	25.36	0.20	417	(111)
44.63	0.19	44.54	0.19	176	(110)
50.63	0.68	13.02	0.17	117	(200)
54.44	0.49	18.53	0.16	30	(242)
74.63	0.59	17.27	0.12	77	(220)

[31] (%PE).

$$\%PE = \left[\left(i_{corr} - i_{(coating)corr}\right)/i_{corr}\right] \times 100$$

i_{corr}, and $i_{(coating)corr}$ are the corrosion current densities values in uncoated and coated, respectively.

Coating type TiO_2/graphite significantly reduced the corrosion current densities, which decreased from 4.3 milliamps per cm^2 for the uncoated DSS to 0.957 milliamps per cm^2 for the coated DSS. Because the coating layer has a lower corrosion rate (CR) than the untreated surface (437.5 mpy), the coating layer has a lower corrosion rate (CR). As previously stated, the corrosion current density of the TiO_2/graphite coated surface is smaller than that of the uncoated surface, and the percent PE is higher on the covered surface than on the uncoated surface. TiO_2/graphite coatings provided better corrosion protection due to the nanoparticles and charged graphite particles adhering to the electrode surface and insulating it from corrosive chemicals [32] such as chloride ions, hydrogen gas and oxygen.

A thin TiO_2/graphite coating applied to the DSS surface in 1 M sulfuric acid solution lowered the cathodic and anodic slopes, implying that a thin protective film on the alloy surface influenced the hydrogen generating mechanisms. As previously stated, it is evident that the hydrogen evolution reaction could be controlled, and the mechanism of the proton discharge reaction [33] varied according to the protective approach used.

The X-ray diffraction peaks of the protective layer's porous alloy surface and crystalline phases were recorded and are summarized in Table 3. The strong peaks at 43.62^0, 50.52^0, and 74.65^0, respectively, can be attributed to the diffraction of (111), (200), and (220) Miller planes, which are characteristic of NiFe elements [34] in DSS alloys with a face-centered cubic (fcc) structure, as illustrated in Fig. 3. Additionally, two weak peaks arise at two values of 44.56^0 and 64.87^0, corresponding to the iron diffraction planes (110) and (200). The products have an fcc-type NiFe matrix within a DSS alloy based on fcc-type Ni,

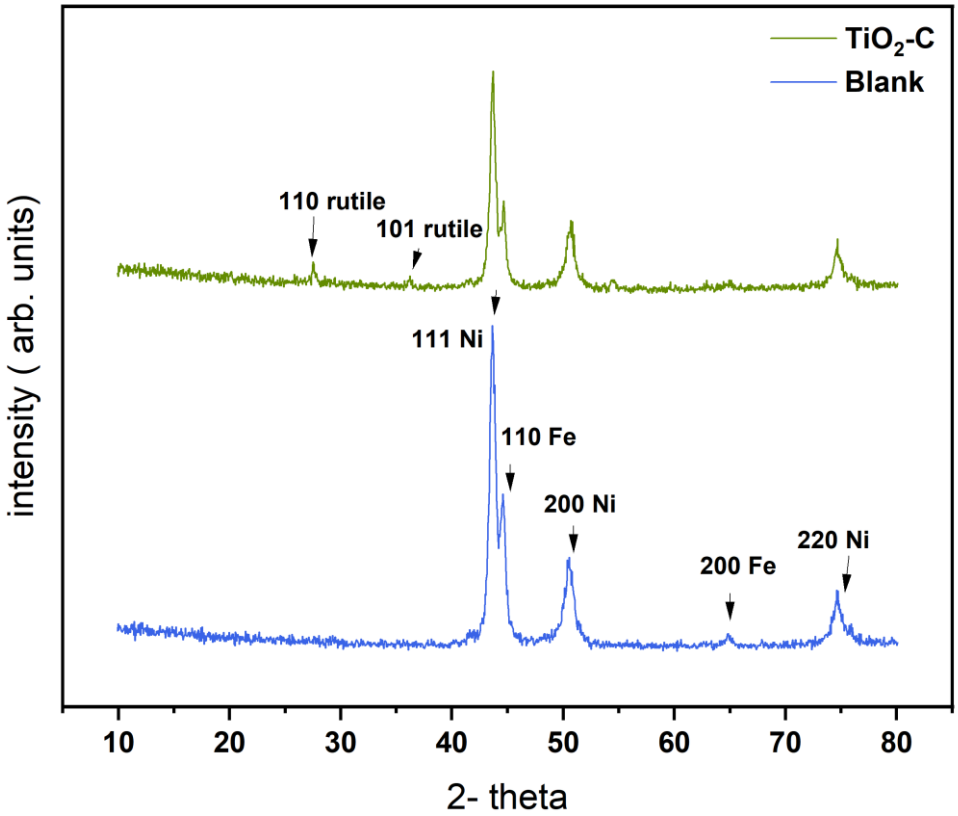

Fig. 3 X-ray diffraction patterns of DSS surface and coating layers of TiO_2/graphite.

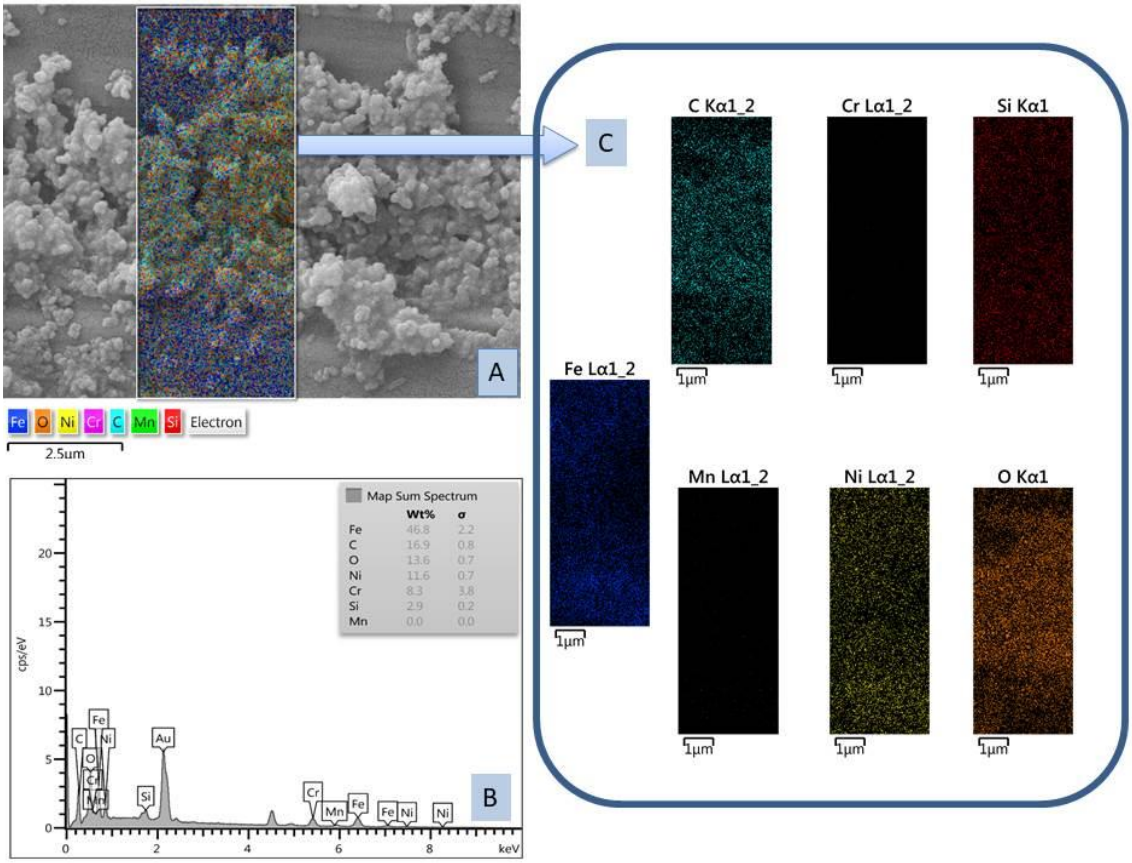

Fig. 4 FESEM image (A), EDX analysis (B), and mapping spectrum (C) of DSS surface

with Fe atoms substituting for some Ni.

A significant concentration of iron atoms in the NiFe matrix is visible in the pattern, indicating that the porous material is composed mostly of iron. The XRD patterns of TiO_2/graphite are depicted in Fig. 3. The diffraction peaks confirmed the thin crystallinity and purity of the coating layers, which showed that there were no diffraction peaks associated with any impurities in the coating layers.

As seen in Table 3, the TiO_2/graphite coating layers contributed to the high diffraction peaks at 27.58^0 and 36.17^0 associated with titanium dioxide's rutile [35-36] phase. The absence of graphite's diffraction peak may be attributable to its integration with TiO^2 at ≈ 27^0 or the reduced graphite concentration in the TiO_2/graphite composite. Additionally, as shown in Table 3, the XRD pattern exhibits the same diffraction peaks as the DSS surface but varying intensities. TiO_2/graphite has an average particle diameter of 23.06 nm. The findings revealed additional differences in the particle sizes of the protective layer formed on the DSS surface by the electrodeposition methodology, indicating that earlier electrochemical approaches revealed a noticeable shift in protection. An EDX spectrum of the uncoated DSS is shown in Fig. 4, along with FESEM images and mapping spectra. Image A shows further cracking layers formed due to corrosion, suggesting that the metal has suffered substantial surface damage due to its breakdown. As illustrated in Fig. 5, the TiO_2/graphite layer that has been created on the DSS surface protects it from corrosion (image A).

It demonstrates that the coatings formed on the DSS alloy surface are more homogeneous and dense than those formed on other surfaces. Because of the density of the deposited layer, there are no cracks or separation of the coatings with obvious superficial cracks. This is due to the high quality of the coating applied. All of these

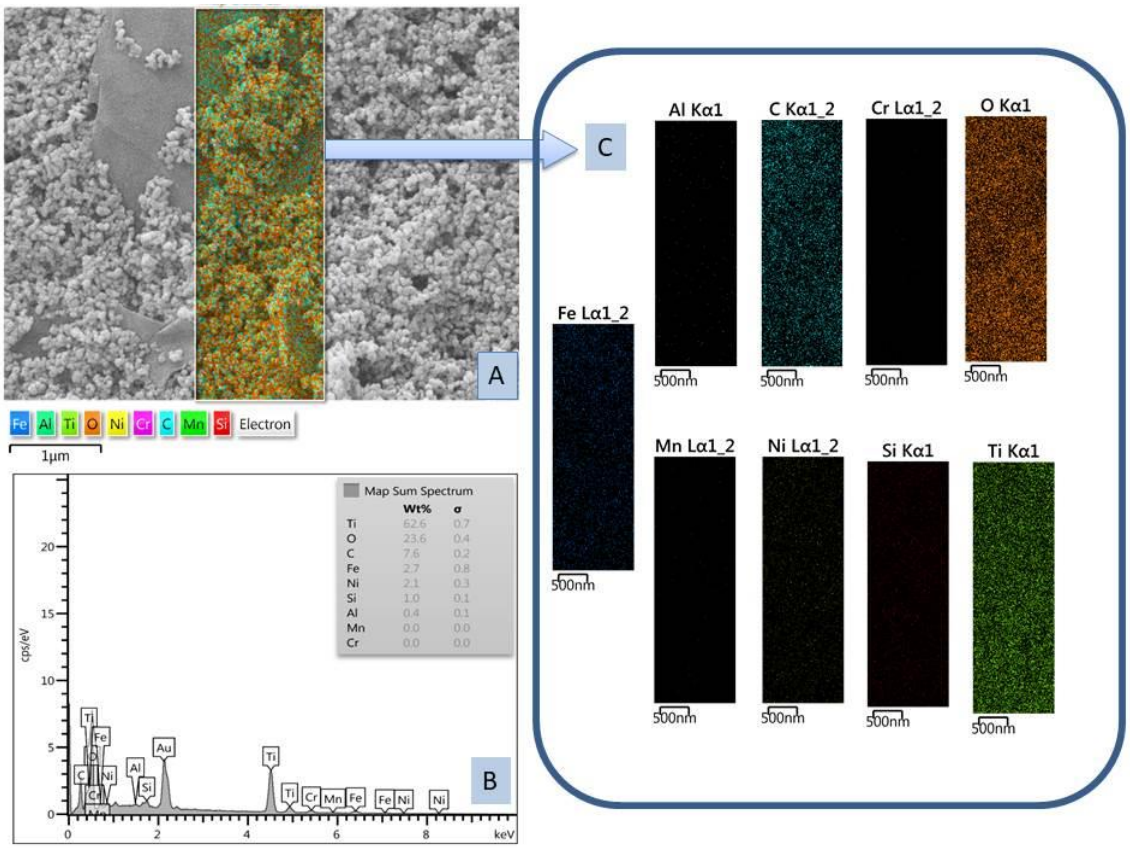

Fig. 5 FESEM image (A), EDX analysis (B), and mapping spectrum (C) of coating layers TiO_2/graphite on the DSS surface.

findings are in agreement with the electrochemical measurements that were taken during the corrosion tests.

The EDS elemental analysis is shown in Fig. B (Fig. 5), which indicates a higher Ti content related to the type of coating layer. Besides, the oxygen and carbon contents were 23.6% and 7.6%, respectively. The iron element content changed from 46.8% to 2.7% in the presence of a TiO_2/graphite coating layer. Besides, the elements were detected by the mapping distribution analysis in the uncoated DSS and TiO_2/graphite related to the contents of components, as shown in image C in Figs. 4 and 5.

CONCLUSION

This work reveals that TiO_2/graphite is an excellent coating effectively formed on a DSS specimen using the electrodeposition method and exhibits excellent corrosion resistance in sulfuric acid solution (1M) saturated with carbon dioxide. Electrochemical tests found that coating the DSS surface with TiO_2 and graphite particles reduced corrosion current densities, resulting in higher polarization resistance in corroded acidic solutions. It takes less time to generate a homogeneous, compact, and adherent TiO_2/graphite coating at high voltage. Electrochemical experiments were utilized to determine the protective layer coating's indirect resistance. Current density and corrosion potential are notably different for the TiO_2/graphite layers than for the DSS sample. The OCP results agree with the potentiodynamic measurements. This study reveals that the TiO_2/graphite coating layer has high corrosion resistance and might be used to protect duplex stainless steel against corrosion in a 1 M H_2SO_4 solution. FESEM confirms these results, corroborated by EDX and mapping examinations and XRD investigations.

ACKNOWLEDGMENT

We thank the Iraqi cement plant in Al-Najaf for

its support in our inquiry. The authors thank the University of Al-Qadisiyah for its cooperation and enabling some measurements.

CONFLICT OF INTEREST

The authors declare that there is no conflict of interests regarding the publication of this manuscript.

REFERENCES

1. Santa-Cruz LA, Machado G, Vicente AA, Hermenegildo TFC, Santos TFA. Effect of high anodic polarization on the passive layer properties of superduplex stainless steel friction stir welds at different chloride electrolyte pH values and temperatures. International Journal of Minerals, Metallurgy, and Materials. 2019;26(6):710-721.
2. Zhu M, Zhang Q, Yuan Y-f, Guo S-y. Effect of microstructure and passive film on corrosion resistance of 2507 super duplex stainless steel prepared by different cooling methods in simulated marine environment. International Journal of Minerals, Metallurgy and Materials. 2020;27(8):1100-1114.
3. Cataldi P, Athanassiou A, Bayer I. Graphene Nanoplatelets-Based Advanced Materials and Recent Progress in Sustainable Applications. Applied Sciences. 2018;8(9):1438.
4. Haran NH, Yousif QA. The efficiency of TiO_2 nanotube photoanode with graphene nanoplatelets as counter electrode for a dye-sensitised solar cell. International Journal of Ambient Energy. 2019;43(1):336-343.
5. Jiang N, Ebadi AG, Kishore KH, Yousif QA, Salmani M. Thermomechanical Reliability Assessment of Solder Joints in a Photovoltaic Module Operated in a Hot Climate. IEEE Transactions on Components, Packaging and Manufacturing Technology. 2020;10(1):160-167.
6. Chan K, Tjong S. Effect of Secondary Phase Precipitation on the Corrosion Behavior of Duplex Stainless Steels. Materials. 2014;7(7):5268-5304.
7. Blay V, Epelde E, Miravalles R, Perea LA. Converting olefins to propene: Ethene to propene and olefin cracking. Catalysis Reviews. 2018;60(2):278-335.
8. Carati A, Ferraris G, Guidotti M, Moretti G, Psaro R, Rizzo C. Preparation and characterisation of mesoporous silica–alumina and silica–titania with a narrow pore size distribution. Catal Today. 2003;77(4):315-323.
9. Paul S, Shrestha S, Lee CM, Harvey MDF. Thermally Sprayed Aluminum (TSA) Coatings for Extended Design Life of 22%Cr Duplex Stainless Steel in Marine Environments. J Therm Spray Technol. 2013;22(2-3):328-336.
10. Velichenko AB, Knysh VA, Luk'yanenko TV, Nikolenko NV. Electrodeposition of PbO2– TiO_2 Nanocomposite Materials from Suspension Electrolytes. Theor Exp Chem. 2016;52(2):127-131.
11. Yousif QA, Al-Zhara AA. Adsorption Aspects, Inhibitory Properties and a Study of Surface Corrosion of Carbon Steel in Acidic Media. Modern Applied Science. 2016;10(10):82.
12. Mahdi KM, Alshamsi HA, Yousif Q. Graphene sheets incorporation in ZnO nanostructure thin film for enhancing the performance of DSSC. Journal of Nanostructures. 2020;10(4):793-801.
13. Nazeer AA, Madkour M. Potential use of smart coatings for corrosion protection of metals and alloys: A review. J Mol Liq. 2018;253:11-22.
14. Liu L, Yu X-M, Zhang B, Meng S-X, Feng Y-Q. Synthesis of nano- TiO_2 assisted by diethylene glycol for use in high efficiency dye-sensitized solar cells. Chin Chem Lett. 2017;28(4):765-770.
15. Zehra S, Mobin M, Aslam J, Parveen M. Assessment of glycine derivative N-benzylidine-2((2-oxo-2-(10H-phenothiazine-10yl)ethyl)amino) acetohydrazide as inhibitor for mild steel corrosion in 1 M HCl solution: electrochemical and theoretical approach. J Adhes Sci Technol. 2017;32(3):317-342.
16. Fadel Z, Yousif QA. (2S,3R)-2-((1-(4-amionophenyl) ethylidene)amino)-3-hydroxybutanoic acid as a novel and eco-friendly corrosion inhibitor for the carbon steel (X56) used in Iraq's oil installations. Journal of Physics: Conference Series. 2020;1664:012093.
17. Uerdingen M, Treber C, Balser M, Schmitt G, Werner C. Corrosion behaviour of ionic liquids. Green Chem. 2005;7(5):321.
18. Raja PB, Sethuraman MG. Inhibition of corrosion of mild steel in sulphuric acid medium by Calotropis procera. Pigment & Resin Technology. 2009;38(1):33-37.
19. Hwang M-J, Kim M-G, Kim S, Kim YC, Seo HW, Cho JK, et al. Cathodic electrophoretic deposition (EPD) of phenylenediamine-modified graphene oxide (GO) for anti-corrosion protection of metal surfaces. Carbon. 2019;142:68-77.
20. Wei J, Gui W, Cui Y, Zhang Z, Yousif QA. SCMNPs@ Uridine/Zn: An efficient and reusable heterogeneous nanocatalyst for the rapid one-pot synthesis of tricyclic fused pyrazolopyranopyrimidine and 3-methyl carboxylate substituted pyrano[2,3-c]pyrazole derivatives under solvent-free conditions. Polish Journal of Chemical Technology. 2020;22(2):20-33.
21. Nine MJ, Cole MA, Tran DNH, Losic D. Graphene: a multipurpose material for protective coatings. Journal of Materials Chemistry A. 2015;3(24):12580-12602.
22. Wen J, Zhang X, Chen J, Liu T, Zhou Y, Li L. Synthesis of 1, 4, 7-triazaheptane derivative and its corrosion inhibition for mild steel in the hydrochloric medium. Journal of Industrial and Engineering Chemistry. 2022;107:333-345.
23. Bensouda Z, El Assiri EH, Sfaira M, Ebn Touhami M, Farah A, Hammouti B. Extraction, Characterization and Anticorrosion Potential of an Essential Oil from Orange Zest as Eco-friendly Inhibitor for Mild Steel in Acidic Solution. Journal of Bio- and Tribo-Corrosion. 2019;5(4).
24. Fadl AM, Sadeek SA, Magdy L, Abdou MI, El-Shiwiniy WH. Multi-functional epoxy composite coating incorporating mixed Cu(II) and Zr(IV) complexes of metformin and 2,2\-bipyridine as intensive network cross-linkers exhibiting anti-corrosion, self-healing and chemical-resistance performances for steel petroleum platforms. Arabian Journal of Chemistry. 2021;14(10):103367.
25. Keerthana L, Sakthivel C, Prabha I. MgO-ZrO_2 mixed nanocomposites: fabrication methods and applications. Materials Today Sustainability. 2019;3-4:100007.
26. WO_3 Nanorods Supported on Mesoporous TiO2 Nanotubes as One-Dimensional Nanocomposites for Rapid Degradation of Methylene Blue under Visible Light Irradiation. American Chemical Society (ACS).
27. Fadel Z, Yousif QA. Inhibitory action of a new derivative of amino acids in aerated acidic media. IOP Conference Series: Earth and Environmental Science. 2021;790(1):012074.
28. Yousif Q, Haran N. Fabrication of TiO_2 nanotubes via three

- electrodes anodization technique under sound waves impact and use in dye-sensitized solar cell. Egyptian Journal of Chemistry. 2020;0(0):0-0.
29. Gomes A, Almeida I, Frade T, Tavares AC. Stability of Zn–Ni–TiO_2 and Zn– TiO_2 nanocomposite coatings in near-neutral sulphate solutions. J Nanopart Res. 2012;14(2).
30. Mir N, Salavati-Niasari M. Photovoltaic properties of corresponding dye sensitized solar cells: Effect of active sites of growth controller on TiO_2 nanostructures. Solar Energy. 2012;86(11):3397-3404.
31. Ahmed SK, Ali WB, Khadom AA. Synthesis and investigations of heterocyclic compounds as corrosion inhibitors for mild steel in hydrochloric acid. International Journal of Industrial Chemistry. 2019;10(2):159-173.
32. Habeeb HJ, Luaibi HM, Dakhil RM, Kadhum AAH, Al-Amiery AA, Gaaz TS. Development of new corrosion inhibitor tested on mild steel supported by electrochemical study. Results in Physics. 2018;8:1260-1267.
33. Lee Y-B, Lee C-H, Lim D-S. The electrical and corrosion properties of carbon nanotube coated 304 stainless steel/polymer composite as PEM fuel cell bipolar plates. Int J Hydrogen Energy. 2009;34(24):9781-9787.
34. Pilarczyk W. The investigation of the structure of bulk metallic glasses before and after laser welding. Cryst Res Technol. 2015;50(9-10):700-704.
35. Pelaez M, Nolan NT, Pillai SC, Seery MK, Falaras P, Kontos AG, et al. A review on the visible light active titanium dioxide photocatalysts for environmental applications. Applied Catalysis B: Environmental. 2012;125:331-349.
36. Yousif QA, Mahdi KM, Alshamsi HA. TiO_2/graphene and MWCNT/PEDOT:PSS nanocomposite-based dye-sensitized solar cell: Design, fabrication, characterization, and investigation. Optik. 2020;219:165294.\